Tetranuclear and Pentanuclear Vanadium(IV/V) Carboxylate Complexes: $[V_4O_8(NO_3)(O_2CR)_4]^{2-}$ and $[V_5O_9X(O_2CR)_4]^{2-}$ ($X = Cl^-$, Br^-) Salts

Gail B. Karet,[†] Ziming Sun,[‡] Dwight D. Heinrich,[†] James K. McCusker,[‡] Kirsten Folting,[†] William E. Streib,[†] John C. Huffman,[†] David N. Hendrickson,*[,‡] and George Christou*[,†]

Department of Chemistry and Molecular Structure Center, Indiana University, Bloomington, Indiana 47405-4001, and Department of Chemistry-0358, University of California at San Diego, La Jolla, California 92093-0358

Received May 22, 1996[⊗]

The syntheses and properties of tetra- and pentanuclear vanadium(IV,V) carboxylate complexes are reported. Reaction of $(NBzEt_3)_2[VOCl_4]$ (**1a**) with NaO_2CPh and atmospheric H_2O/O_2 in MeCN leads to formation of $(NBzEt_3)_2[V_5O_9Cl(O_2CPh)_4]$ **4a**; a similar reaction employing $(NEt_4)_2[VOCl_4]$ (**1b**) gives $(NEt_4)_2[V_5O_9Cl(O_2CPh)_4]$ (**4b**). Complex **4a**·MeCN crystallizes in space group $P2_12_12_1$ with the following unit cell dimensions at −148 °C: $a = 13.863(13)$ Å, $b = 34.009(43)$ Å, $c = 12.773(11)$ Å, and $Z = 4$. The reaction between $(NEt_4)_2[VOBr_4]$ (**2a**) and NaO_2CPh under similar conditions gives $(NEt_4)_2[V_5O_9Br(O_2CPh)_4]$ (**6a**), and the use of $(PPh_4)_2[VOBr_4]$ (**2b**) likewise gives $(PPh_4)_2[V_5O_9Br(O_2CPh)_4]$ (**6b**). Complex **6b** crystallizes in space group $P2_12_12_1$ with the following unit cell dimensions at −139 °C: $a = 18.638(3)$ Å, $b = 23.557(4)$ Å, $c = 12.731(2)$ Å, and $Z = 4$. The anions of **4a** and **6b** consist of a V_5 square pyramid with each vertical face bridged by a μ_3-O^{2-} ion, the basal face bridged by a μ_4-X^- (X = Cl, Br) ion, and a terminal, multiply-bonded O^{2-} ion on each metal. The RCO_2^- groups bridge each basal edge to give C_{4v} virtual symmetry. The apical and basal metals are V^V and V^{IV}, respectively (i.e., the anions are trapped-valence). The reaction of **1b** with $AgNO_3$ and Na(tca) (tca = thiophene-2-carboxylate) in MeCN under anaerobic conditions gives $(NEt_4)_2[V_4O_8(NO_3)(tca)_4]$ (**7**). Complex **7**·H_2O crystallizes in space group $C2/c$ with the following unit cell dimensions at −170 °C: $a = 23.606(4)$ Å, $b = 15.211(3)$ Å, $c = 23.999(5)$ Å, and $Z = 4$. The anion of **7** is similar to those of **4a** and **6b** except that the apical [VO] unit is absent, leaving a V_4 square unit, and the μ_4-X^- ion is replaced with a μ_4,η^1-NO_3^- ion. The four metal centers are now at the V^{IV}, $3V^V$ oxidation level, but the structure indicates four equivalent V centers, suggesting an electronically delocalized system. Variable-temperature magnetic susceptibility data were collected on powdered samples of **4b**, **6a**, and **7** in the 2.00−300 K range in a 10 kG applied field. **4b** and **6a** both show a slow increase in effective magnetic moment (μ_{eff}) from ∼3.6−3.7 μ_B at 320 K to ∼4.5−4.6 μ_B at 11.0 K and then a slight decrease to ∼4.2 μ_B at 2.00 K. The data were fit to the theoretical expression for a $V^{IV}{}_4$ square with two exchange parameters $J = J_{cis}$ and $J' = J_{trans}$ ($\hat{H} = -2JS_iS_j$): fitting of the data gave, in the format **4b**/**6a**, $J = +39.7/+46.4$ cm^{-1}, $J' = -11.1/-18.2$ cm^{-1} and $g = 1.83/1.90$, with the complexes possessing $S_T = 2$ ground states. The latter were confirmed by magnetization *vs* field studies in the 2.00−30.0 K and 0.500−50.0 kG ranges: fitting of the data gave $S_T = 2$ and $D = 0.00$ cm^{-1} for both complexes, where D is the axial zero-field splitting parameter. Complex **7** shows a nearly temperature-independent μ_{eff} (1.6−2.0 μ_B) consistent with a single d electron per V_4 unit. The ^{1}H NMR spectra of **4b** and **6a** in CD_3CN are consistent with retention of their pentanuclear structure on dissolution. The EPR spectrum of **7** in a toluene/MeCN (1:2) solution at ∼25 °C yields an isotropic signal with a 29-line hyperfine pattern assignable to hyperfine interactions with four equivalent $I = {}^7/_2$ ^{51}V nuclei.

Introduction

Vanadium chemistry is of relevance to a number of important industrial processes such as the refining of crude oils by the petroleum industry. Heavy crude oils with large amounts of organic sulfur compounds (thiophenes, thiols, and disulfides) also have significant amounts of metallic impurities, chiefly V, Ni, and Fe.[1] The oil-soluble vanadyl species are reduced and sulfided and deposited on the catalyst as insoluble vanadium sulfides, which decrease the activity of the catalyst pores.[1a,2] The molecular mechanism for vanadium deposition on the catalyst as vanadium sulfides (chiefly V_2S_3 and V_3S_4) is not completely understood, although it has been extensively studied.[1a,3−5] As part of our own efforts, we have prepared a variety of discrete V/S compounds with thiolate/sulfide/persulfide ligands to model the V/S intermediates to V_2S_3/V_3S_4 that form under the reducing and S-rich conditions of hydrodesulfurization.[6,7]

[†] Indiana University.
[‡] University of California at San Diego.
[⊗] Abstract published in *Advance ACS Abstracts,* October 1, 1996.

(1) (a) *Metal Complexes in Fossil Fuels*; Filby, R. H., Branthaver, J. F., Eds.; *ACS Symposium Series* 344; *American Chemical Society: Washington, DC,* **1987**. (b) Yen, T. F. *The Role of Trace Metals in Petroleum,* Ann Arbor Science: Ann Arbor, MI, 1975.
(2) (a) Ware, R. A.; Wei, J. *J. Catal.* **1985**, *93*, 100, 122, and 125. (b) Speight, J. G. *The Desulfurization of Heavy Crudes and Residues*; Marcel Dekker: New York, 1981.
(3) Toulhout, H.; Szymanski, R.; Plumail, J. C. *Catal. Today* **1990**, *7*, 531.
(4) (a) Reynolds, J. G.; Biggs, W. R. *Fuel. Sci. Technol. Int.* **1986**, *4*, 593. (b) Reynolds, J. G.; Gallegos, E. J.; Fish, R. H.; Komlenic, J. J. *Energy Fuels* **1987**, *1*, 36. (c) Dickson, F. E.; Petrakis, L. *Anal. Chem.* **1974**, *44*, 1129. (d) Reynolds, J. G. *Liq. Fuels Technol.* **1985**, *3*, 73.
(5) (a) Loos, M.; Ascone, I.; Goulon-Ginet, C.; Goulon, J.; Guillard, C.; Lacroix, M.; Breysse, M.; Faure, D.; Des Courieves, T. *Catal. Today* **1990**, *7*, 515. (b) Silbernagel, B. G. *J. Catal.* **1979**, *56*, 315. (c) Silbernagel, B. G.; Mohan, R. R.; Singhal, G. H. *ACS Symp. Ser.* **1984**, No. *248*, 91.

S0020-1669(96)00593-9 CCC: $12.00

Vanadium−oxygen species are also of industrial relevance. Vanadium pyrophosphate, $(VO)_2P_2O_7$, catalyzes the oxidation of *n*-butane to maleic anhydride under mild conditions,[8] and many vanadium phosphates and organophosphates have thus been synthesized hydrothermally.[9,10] The oxide V_2O_5 is useful as a reagent for organic synthesis; it catalyzes the oxidation of furfural by $NaClO_3$ to form fumaric acid, the oxidation of hydroquinone to quinone, and the oxidation of cyclic ketones or alcohols to dicarboxylic acids.[11] An important industrial V_2O_5-catalyzed reaction is the O_2 oxidation of SO_2 to SO_3, which is then converted to H_2SO_4.[12] The catalytically-active phase is thought to be a liquid, and V_2O_5 is activated by the addition of alkali metal salts such as K_2SO_4 or $K_2S_2O_7$.[12] The liquid phase of K-activated V_2O_5 catalysts contains small ions and aggregates such as K^+, VO_2^+, VO^{3+}, $V_2O_2^{4+}$, SO_4^{2-}, and $S_2O_7^{2-}$.[12] Several mechanisms have been proposed for this reaction, many of which involve adduct formation between the VO^{n+} species and sulfur oxides, but the rate-determining step has not been identified.[12]

As an extension to our V/S studies, therefore, we have become interested in V/O chemistry, specifically that involving soluble clusters with carboxylates as peripheral ligands. Most V carboxylates currently known are trinuclear or smaller: the most common structural type comprises a triangular $[V_3O]$ unit with a central μ_3-O^{2-} ion and has been obtained at several oxidation levels.[13] Also known are the linear trinuclear species $[V_3(O_2CR)_6(tmeda)_2]$ (R = $PhCH_2$, Ph_2CH) prepared from the reaction of $V(tmeda)_2Cl_2$ with carboxylic acids.[14] Only a handful of V carboxylate complexes with metal nuclearities >3 have been prepared, such as $[V_4O_8(C_2O_4)_4(H_2O)_2]^{4-}$,[15] $[KV_4O_8(O_2CR)_4]$-(O_2CR) (R = Bu^tCH_2),[16] $[V_6O_{10}(O_2CPh)_9]$,[17a] $[H_6V_{10}O_{22}$-$(RCO_2)_6]^{2-}$,[17b] and $[V_4Zn_4(O_2CPh)_{12}(THF)_4]$.[18] Our own work, in addition to $[V_4O_2(O_2CEt)_7(bpy)_2](ClO_4)$,[19] has contributed $[V_4O_8(NO_3)(O_2CR)_4]^{2-}$ and $[V_5O_9Cl(O_2CR)_4]^{2-}$ salts,[20] and the former has more recently been reported by others at a higher oxidation level *viz* $[V_4O_8(NO_3)(O_2CR)_4]^-$.[21] We herein describe in detail the syntheses and crystal structures of $[V_5O_9X(O_2CR)_4]^{2-}$ (X = Cl, Br) and $[V_4O_8(NO_3)(O_2CR)_4]^{2-}$ salts, together with their electrochemical, magnetochemical, and spectroscopic properties.

Experimental Section

All manipulations were carried out under an inert atmosphere using standard Schlenk and glovebox techniques, unless otherwise noted. All solvents were dried and degassed by standard methods except where indicated otherwise: MeCN was distilled from 4 Å molecular sieves, and Et_2O and toluene were distilled from sodium/benzophenone. $(NBzEt_3)_2[VOCl_4]$ (**1a**) and $(NEt_4)_2[VOCl_4]$ (**1b**) were prepared as described elsewhere,[20,22] and $Na(O_2CPh$-*p*-Me) and Na(tca) (tca = thiophone-2-carboxylate) were made from the corresponding acid and NaOEt in EtOH. $AgNO_3$, EtOH, and NaO_2CPh were used as received.

$(NEt_4)_2[VOBr_4]$ (2a). A slurry of $VOSO_4 \cdot 2H_2O$ (5.0 g, 25 mmol), LiBr (4.3 g, 50 mmol), and NEt_4Br (10.5 g, 50 mmol) in EtOH (50 mL) was maintained at reflux for 3 h, and the resultant blue solution was cooled to room temperature. It was then stirred overnight at room temperature and concentrated to dryness under dynamic vacuum. The remaining EtOH was removed by two cycles of dissolution of the residue in MeCN (30 mL), followed by removal of the solvent *in vacuo*. The solid was then dissolved in MeCN (60 mL), the green solution was filtered to remove Li_2SO_4, and the filtrate was concentrated to ∼25 mL and stored at −10 °C overnight. Green crystals of **2a** were collected in 41% yield (6.6 g). $(PPh_4)_2[VOBr_4]$ **(2b)** was prepared in an analogous manner employing PPh_4Br.

$(NBzEt_3)_2[V_5O_9Cl(O_2CPh)_4]$ (4a). To a light green solution of $(NBzEt_3)_2[VOCl_4]$ (**1a**) (1.17 g, 1.97 mmol) in MeCN (100 mL) was added NaO_2CPh (0.575 g, 3.99 mmol). The resulting solution was exposed briefly to air (1-3 min), the flask resealed, and the solution stirred for 30 min. The deep green solution was filtered, and the filtrate allowed to slowly evaporate, giving large deep green crystals in 56% yield. Dried solid analyzed as solvent-free. Anal. Calcd (found) for $C_{54}H_{64}N_2O_{17}ClV_5$: C, 49.77 (49.4); H, 4.95 (5.12); N, 2.15 (2.57). Crystals of **4a**·MeCN suitable for crystallography were grown by slow diffusion of Et_2O into a solution of **4a** in MeCN. $(NEt_4)_2[V_5O_9Cl(O_2$-$CPh)_4]$ (**4b**) was made in an analogous manner starting from $(NEt_4)_2$-$[VOCl_4]$ (**1b**). Electronic spectrum in MeCN, λ_{max}, nm (ϵ_M, L mol^{-1} cm^{-1}): 314 (3600), ∼402 (sh, 810), 590 (220), 762 (320).

$(NEt_4)_2[V_5O_9Cl(O_2CPh$-*p*-$Me)_4]$ (5). This was prepared from complex **1b** and $Na(O_2CPh$-*p*-Me) by a method analogous to that for **4a** and **4b**. The yield of complex **5** was 32%. Anal. Calcd (found) for $C_{48}H_{68}N_2O_{17}ClV_5$: C, 46.65 (46.29); H, 5.56 (5.28); N, 2.27 (2.39).

$(NEt_4)_2[V_5O_9Br(O_2CPh)_4]$ (6a). To a stirred solution of complex **2a** (2.58 g, 3.98 mmol) in MeCN (50 mL) was added NaO_2CPh (1.12 g, 7.77 mmol). The solution was exposed to air for *ca*. 5 min and the flask was then resealed and stirred at room temprature for 2 h, during which time the solution turned slightly deeper green. The green solution was filtered to remove NaBr, and the filtrate layered with Et_2O. After several days, the green crystals that had formed were collected by filtration, washed with a little Et_2O, and dried *in vacuo*. The yield was 25% (0.30 g). Selected IR data (Nujol), cm^{-1}: 1595 (s), 1552 (s), 999 (s), 972 (s). Anal. Calcd (found) for $C_{46}H_{65}N_3O_{18}BrV_5$ (**6a**·MeCN·H_2O): C, 43.08 (42.86); H, 5.11 (5.65); N, 3.28 (3.12). The complex $(PPh_4)_2[V_5O_9Br(O_2CPh)_4]$ (**6b**) was prepared similarly using

(6) (a) Money, J. K.; Huffman, J. C.; Christou, G. *Inorg. Chem.* **1985**, *24*, 3297. (b) Money, J. K.; Folting, K.; Huffman, J. C.; Collison, D.; Temperly, J.; Mabbs, F. E.; Christou, G. *Inorg. Chem.* **1986**, *25*, 4583. (c) Money, J. K.; Huffman, J. C.; Christou, G. *J. Am. Chem. Soc.* **1987**, *109*, 2210. (d) Money, J. K.; Folting, K.; Huffman, J. C.; Christou, G. *Inorg. Chem.* **1987**, *26*, 944. (e) Money, J. K.; Huffman, J. C.; Christou, G. *Inorg. Chem.* **1988**, *27*, 507.

(7) (a) Castro, S. L.; Martin, J. D.; Christou, G. *Inorg. Chem.* **1993**, *32*, 2978. (b) Sendlinger, S. C.; Nicholson, J. R.; Lobkovsky, E. B.; Huffman, J. C.; Rehder, D.; Christou, G. *Inorg. Chem.* **1993**, *32*, 204. (c) Dean, N. S.; Bartley, S. L.; Stgreib, W. E.; Lobkovsky, E. B.; Christou, G. *Inorg. Chem.* **1995**, *34*, 1608. (d) Reynolds, J. G.; Sendlinger, S. C.; Murray, A. M.; Huffman, J. C.; Christou, G. *Angew. Chem., Int. Ed. Engl.* **1992**, *31*, 1253.

(8) (a) Seeboth, H.; Freiburg, H.-J.; Hopf, G.; Kressig, J.; Kubias, B.; Ladwig, G.; Lucke, B.; Muller, G.; Wolf, H., DDR Patent 113 210, 1975. (b) Seeboth, H.; Kubias, B.; Wolf, H.; Lucke, B. *Chem. Technol.* **1976**, *28*, 730.

(9) (a) Soghomonian, V.; Chen, Q.; Haushalter, R. C.; Zubieta, J.; O'Connor, C. J. *Science* **1993**, *259*, 1596. (b) Soghomonian, V.; Chen, Q.; Haushalter, R. C.; Zubieta, J. *Angew. Chem., Int. Ed. Engl.* **1993**, *32*, 610. (c) Khan, M. I.; Lee, Y.-S.; O'Connor, C. J.; Haushalter, R. C.; Zubieta, J. *Inorg. Chem.* **1994**, *33*, 3855.

(10) (a) Vaughey, J. T.; Harrison, W. T. A.; Jacobson, A. J.; Goshorn, D. P.; Johnson, J. W. *Inorg. Chem.* **1994**, *33*, 2481. (b) Huan, G.; Day, V. W.; Jacobson, A. J.; Goshorn, D. P. *J. Am. Chem. Soc.* **1991**, *113*, 3188. (c) Johnson, J. W.; Jacobson, A. J.; Brody, J. F.; Lewandowski, J. T. *Inorg. Chem.* **1984**, *23*, 3844.

(11) Fieser, L. F.; Fieser, M. *Reagents for Organic Synthesis*; Wiley: New York, 1967; pp 733, 1057, and references therein.

(12) Urbanek, A.; Trela, M. *Catal. Rev.−Sci. Eng.* **1980**, *21*, 73.

(13) (a) Cotton, F. A.; Lewis, G. E.; Mott, G. N. *Inorg. Chem.* **1982**, *21*, 3127. (b) Cotton, F. A.; Lewis, G. E.; Mott, G. N. *Inorg. Chem.* **1982**, *21*, 3316. (c) Cotton, F. A.; Wang, W. *Inorg. Chem.* **1982**, *21*, 2675. (d) Cotton, F. A.; Extine, M. W.; Falvello, L. R.; Lewis, D. B.; Lewis, G. E.; Murillo, C. A.; Schwotzer, W.; Tomas, M.; Troup, S. M. *Inorg. Chem.* **1986**, *25*, 3505. (e) Castro, S. L.; Streib, W. E.; Sun, S.-J.; Christou, G. *Inorg. Chem.*, submitted for publication.

(14) Edema, J. J. H.; Gambarotta, S.; Hao, S.; Bensimon, C. *Inorg. Chem.* **1991**, *30*, 2584.

(15) Rieskamp, H.; Gietz, P.; Mattes, R. *Chem. Ber.* **1976**, *109*, 2090.

(16) Priebsch, W.; Rehder, D.; von Oeynhausen, M. *Chem. Ber.* **1991**, *124*, 761.

(17) (a) Rehder, D.; Priebsch, W.; von Oeynhausen, M. *Angew. Chem., Int. Ed. Engl.* **1989**, *28*, 1221. (b) Muller, A.; Rohlfing, R.; Krickemeyer, E.; Bogge, H. *Angew. Chem., Int. Ed. Engl.* **1993**, *32*, 909.

(18) Cotton, F. A.; Duraj, S. A.; Roth, W. J. *Inorg. Chem.* **1984**, *23*, 4042.

(19) Castro, S. L.; Sun, Z.; Bollinger, J. C.; Hendrickson, D. N.; Christou, G. *J. Chem. Soc., Chem. Commun.* **1995**, 2517.

(20) Heinrich, D. D.; Folting, K.; Streib, W. E.; Huffman, J. C.; Christou, G. *J. Chem. Soc., Chem. Commun.* **1989**, 1411.

(21) Arrowsmith, S.; Dove, M. F. A.; Logan, N.; Antipin, M. Y. *J. Chem. Soc., Chem. Commun.* **1995**, 627.

(22) Rambo, J. R. Ph.D. Thesis, Indiana University, 1993.

Table 1. Crystallographic Data for Complexes **4a**·MeCN, **6b**, and **7**·H_2O

	4a·MeCN	**6b**	**7**·H_2O
formula[a]	$C_{56}H_{67}ClN_3O_{17}V_5$	$C_{76}H_{60}O_{17}P_2BrV_5$	$C_{36}H_{54}N_3O_{20}S_4V_4$
fw[a]	1344.31	1641.86	1180.84
space group	$P_12_12_1$	$C2/c$	$P2_12_12_1$
a, Å	13.863(13)	23.606(4)	18.638(3)
b, Å	34.009(43)	15.211(3)	23.557(4)
c, Å	12.773(11)	23.999(5)	12.731(2)
β, deg	90	127.60(1)	90
V, Å^3	6021.9	6827.0	5589.7
Z	4	4	4
T, °C	−148	−170	−139
radiation, Å[b]	0.71069	0.71069	0.71069
ϱ_{calc}, g/cm^3	1.438	1.597	1.403
μ, cm^{-1}	8.324	13.335	8.353
no. of unique data	7862	6047	4459
R_{merge}	0.056	0.048	0.022
no. of obsd data[c]	6053	4804	2947
R[d] (R_w[e])	6.02 (5.47)	4.91 (4.49)	9.47 (9.53)

[a] Including solvate molecules. [b] Graphite monochromator. [c] $F > 3\sigma(F)$. [d] $R = \sum||F_o| - F_c||/\sum|F_o|$. [e] $R_w = [\sum w(|F_o| - |F_c|)^2/\sum w|F_o|^2]^{1/2}$ where $w = 1/\sigma^2(|F_o|)$.

$(PPh_4)_2[VOBr_4]$, and was employed for the crystallographic studies. Electronic spectrum in MeCN, λ_{max}, nm (ϵ_M, L mol^{-1} cm^{-1}): 312 (2600), 382 (sh, 800), 592 (250), 768 (290).

$(NEt_4)_2[V_4O_8(NO_3)(tca)_4]$ (7). To a solution of complex **1b** (0.94 g, 2.0 mmol) in undried, degassed MeCN (50 mL) under an inert atmosphere was added $AgNO_3$ (1.32 g, 7.77 mmol). This gave a rapid precipitate of AgCl and produced a blue solution. To the latter was added solid Na(tca) (0.62 g, 4.1 mmol) and the mixture stirred; within a few minutes, a dark green solution was obtained. This was filtered, the volume of the filtrate reduced to ∼20 mL under vacuum, and the flask stored at room temperature for two days to give dark green crystals in 40% yield. Anal. Calcd (found) for $C_{36}H_{54}N_3O_{20}S_4V_4$ (**7**·H_2O): C, 36.6 (36.8); H, 4.6 (4.7); N, 3.6 (3.7); S, 10.9 (10.4); V, 17.3 (17.2). The electronic spectrum in MeCN showed no well-defined maxima in the 360−800 nm range.

X-ray Crystallography and Structure Solution. Details of the diffractometry, low-temperature facilities, and computational procedures employed by the Molecular Structure Center are available elsewhere.[23a] Suitable dark green crystals of **4a**·MeCN, **6b**, and **7**·H_2O were chosen from samples examined in a N_2 glovebag, attached to glass fibers with silicone grease, and transferred to the cold stream of a Picker four-circle diffractometer. Data collection parameters ($6° \le 2\theta \le 45°$) are summarized in Table 1. The structures were solved by a combination of direct methods (MULTAN) and Fourier techniques and refined by full-matrix least-squares cycles. The octants collected were $+h$, $+k$, $+l$ for **4** and **7**, and $+h$, $\pm k$, $\pm$l for **6b**.

For **4a**·MeCN, a systematic search of a limited hemisphere of reciprocal space yielded a set of reflections that exhibited orthorhombic symmetry. The systematic extinction of $h00$ for $h = 2n + 1$, $0k0$ for $k = 2n + 1$, and 001 for $l = 2n + 1$ uniquely identified the space group as the non-centrosymmetric $P2_12_12_1$. Four standards monitored every 300 reflections showed no systematic trends. The five V atoms and the Cl atom were located in the initial MULTAN E-map, and the remaining non-hydrogen atoms were located in successive difference Fourier maps phased on the already-located atoms. All of the hydrogen atoms, except for those on the MeCN molecule in the lattice, were introduced in fixed, calculated positions. All non-hydrogen atoms were refined anisotropically. No absorption correction was applied. The largest peak in the final difference Fourier map was 0.61 e/Å^3. The obtained structure was the correct absolute structure; refining the other enantiomer gave R (R_w) = 0.0650 (0.600).

For **6b**, a systematic search of a limited hemisphere of reciprocal space yielded a set of reflections that revealed a C-centered monoclinic cell. Following complete data collection, the additional condition $l = 2n$ for $h0l$ indicated the space group to be Cc or $C2/c$; the choice of the latter was proven correct by subsequent successful solution of the structure. Four standards monitored every 300 reflections showed no systematic trends. The five V and one Br atoms were located from an initial E-map, and the remaining non-hydrogen atoms were located in successive difference Fourier maps phased on the already-located atoms. No disorder problems were encountered. All non-hydrogen atoms were refined with anisotropic thermal parameters. Hydrogen atoms were included in fixed, calculated positions with thermal parameters fixed at one plus the equivalent isotropic thermal parameter of the C atoms to which they were attached. An absorption correction was applied using the program AGNOST.[23b] The largest peak in the final difference Fourier map was 0.74 e/Å^3 near the Br atom.

For complex **7**·H_2O, data collection was undertaken at −139 °C because fragmentation of the crystal occurred at lower temperatures. A search of a limited hemisphere of reciprocal space revealed a set of reflections with orthorhombic symmetry and indicated the space group as non-centrosymmetric $P2_12_12_1$. The four V atoms were located from the initial E-map, and the rest of the non-hydrogen atoms were observed in successive difference Fourier maps. The compound exhibited very high thermal motion, and the S atoms of the thiophene groups were disordered about two positions. In three of the thiophene rings, the disorder was settled by varying the occupancies; in the fourth, at C(30), two positions were found for C(35) and C(36). The two NEt_4^+ cations also showed very high thermal motion. In addition, two peaks were located within 1.8 Å of each other and were presumed to be disordered solvent or water molecules. They were assigned oxygen scattering factors, and the occupancies were refined to 0.75. Hydrogen atoms were not located or included. All of the non-hydrogen atoms except for those on the disordered thiophene ring at C(30) and the two "solvent" atoms were refined anisotropically. No absorption correction was performed. Because of the poor quality of the data, due to solvent loss or other factors, it was not possible to determine the absolute structure for this noncentrosymmetric space group. The largest peak in the final difference map was 0.6 e/Å^3.

Physical Measurements. NMR spectra were recorded in CD_3CN on a Varian XL300 spectrometer; the solvent was used as an internal NMR reference. Chemical shifts are quoted on the δ scale (downfield shifts are positive). EPR measurements were performed at X-band frequencies (9.4 GHz) on a Bruker ESP300D spectrometer with a Hewlett-Packard 5350B microwave frequency counter and an Oxford liquid He cryostat and temperature controller. Electronic spectra were recorded on a Hewlett-Packard Model 8452A spectrophotometer. Variable-temperature magnetic susceptibility data for powdered samples (restrained in Vaseline to prevent torquing) were recorded in the temperature range 5−320 K and at an applied field of 10 kG on a D.C. SQUID susceptometer. Data were also collected in the temperature range 2−30 K at applied fields of 0.5−50 kG. Diamagnetic corrections, estimated from Pascal's constants, were subtracted from the experimental susceptiblities to give the molar paramagnetic susceptiblities.

Results

Syntheses. The synthetic procedure to the tetra- and pentanuclear complexes described all involve controlled oxidation/hydrolysis reactions of the anions $[VOX_4]^{2-}$ in organic solvents in the presence of NaO_2CR. Reaction of $[VOCl_4]^{2-}$ salts with NaO_2CR (R = C_4H_3S, Ph) in MeCN with brief exposure to air yields deep green solutions from which can be isolated salts of the $[V_5O_9Cl(O_2CR)_4]^{2-}$ anions. The precise length of air exposure is not critical since the product is not itself very air-sensitive, and we have found this procedure to be a convenient and readily reproducible route to these anions. Extensive air exposure leads to V/O products with no RCO_2^- ligands (as judged by IR). Thus, V/O/RCO_2 products represent the result of partial hydrolysis of $[VOCl_4]^{2-}$ in the presence of NaO_2-CPh. Our original work was performed with $NaO_2CC_4H_3S$ (tca, thiophene-2-carboxylate) and yielded $(NBzEt_3)_2[V_5O_9Cl(tca)_4]$ **3** whose crystal structure was reported.[20] However, the latter was complicated by disorder problems in the thiophene group,

(23) (a) Chisholm, M. H.; Folting, K.; Huffman, J. C.; Kirkpatrick, C. C. *Inorg. Chem.* **1984**, *23*, 1021. (b) de Meulenaer, J.; Tompa, H. *Acta Crystallogr.* **1965**, *19*, 1014.

and this carboxylate is also not the most suitable for ^{1}H NMR studies. We have since instead employed NaO_2CPh and found that this also readily gives $(NR_4)_2[V_5O_9Cl(O_2CPh)_4]$ (R_4 = $BzEt_3$, **4a**, or Et_4, **4b**); complex **3** will thus not be discussed further.

The formulation of the anion of **4** requires a $4V^{IV},V^V$ oxidation state description, indicating an increase in both the O^{2-}:V ratio and metal oxidation state *vis-à-vis* the $VOCl_4^{2-}$ (V^{IV}) starting material, thus rationalizing the need for exposure of the reaction mixture to air. The formation of the anion of **4** is undoubtedly facilitated by the ability of carboxylate groups to function as H^+ acceptors during the incorporation of H_2O-derived oxide ions into the $[V_5O_9Cl]$ core. The RCO_2^-:$[VOCl_4]^{2-}$ ratio of 2:1 was found to be optimum; an increase in this ratio gave impure material. The synthetic procedure to **4** could undoubtedly be extended to a variety of substituted-benzoate derivatives; use of Na(*p*-methylbenzoate) in a smaller scale reaction gave $(NEt_4)_2[V_5O_9Cl(O_2CPh\text{-}p\text{-}Me)_4]$ (**5**), required to assist the ^{1}H NMR studies (*vide infra*).

The procedure to complex **4** was also successfully employed for the preparation of the Br^- analogue $[V_5O_9Br(O_2CPh)_4]^{2-}$, the anion of **6**, by substitution of complex **2** for **1** (i.e. $[VOBr_4]^{2-}$ for $[VOCl_4]^{2-}$), and this was structurally characterized as the PPh_4^+ salt (**6b**). This anion is again at the $4V^{IV},V^V$ oxidation level and is essentially isostructural with the Cl^- analogue (*vide infra*).

The occurrence of rare, tetragonal pyramidal μ_4-halide ions in complexes **3**−**6** was noteworthy and it became of interest to ask whether halide-free versions might be accessible. Preliminary attempts to abstract Cl^- with $AgNO_3$ from preformed $[V_5O_9Cl(O_2CR)_4]^{2-}$ anions did not give pure product(s), and $AgNO_3$ was instead added to the reaction mixture to precipitate Cl^- as AgCl. For the tca^- reaction, the isolated product was $(NEt_4)_2[V_4O_8(NO_3)(tca)_4]$ (**7**) instead of **3**; we were unable to obtain pure products with $PhCO_2^-$, and our studies to-date have thus been concentrated on the tca^- complex **7**. Clearly, the identity of the product has altered *vis-à-vis* **3**−**6**, both in metal nuclearity and oxidation level; **7** is $V^{IV},3V^V$. These differences probably result from a combination of factors, including the absence of Cl^- and the presence of potentially-oxidizing Ag^+, and delineation of the relative importance of these and other factors is being addressed in more detail in further studies, including the use of Tl^+ reagents. However, it is important to note that the absence of halide ions has not resulted in the corresponding absence of a μ_4-ion bridging the V_4 square; instead, a NO_3^- ion has taken up this role (*vide infra*). Complex **7** is much more air-sensitive than **3**−**6** and in solution must be handled under an inert atmosphere.

The formation of complexes **3**−**7** by partial hydrolysis of $[VOX_4]^{2-}$/NaO_2CR mixtures parallels the preparative procedures to a number of other V/O/RCO_2 complexes in organic solvents. For example, dinuclear $[V_2O(O_2CR)_2]^{2+}$-, triangular $[V_3O]^{z+}$-, and cubic $[V_4O_4]^{4+}$-containing complexes may be obtained from non-oxide V^{II} or V^{III} reagents.[13,24] The source of the oxide ligands in $[KV_4O_8(O_2CCH_2Bu^t)_4](O_2CCH_2Bu^t)$ is also H_2O (or O_2).[16] The H^+-acceptor property of RCO_2^- groups is probably important to some extent in all of these transformations in organic solvents.

Description of Structures. ORTEP plots of the anions of **4a**, **6b**, and **7** are given in Figures 1−4; space-filling diagrams viewed approximately along the C_4 axes are presented in Figure 5. Selected fractional coordinates and pertinent interatomic distances and angles are listed in Tables 2−7.

(24) Köppen, M.; Fresen, G.; Wieghardt, K.; Llusar, R. M.; Nuber, B.; Weiss, J. *Inorg. Chem.* **1988**, *27*, 721.

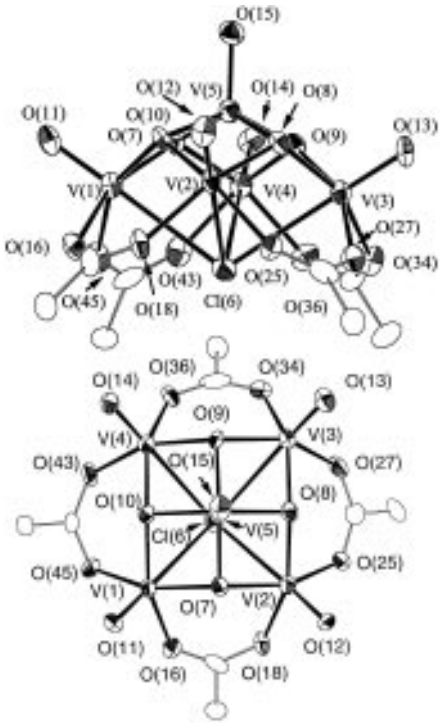

Figure 1. ORTEP representation at the 50% probability level of the $[V_5O_9Cl(O_2CPh)_4]^{2-}$ anion of **4a**, showing only one C atom of each Ph ring: (top) side view, and (bottom) top view approximately along the virtual C_4 axis.

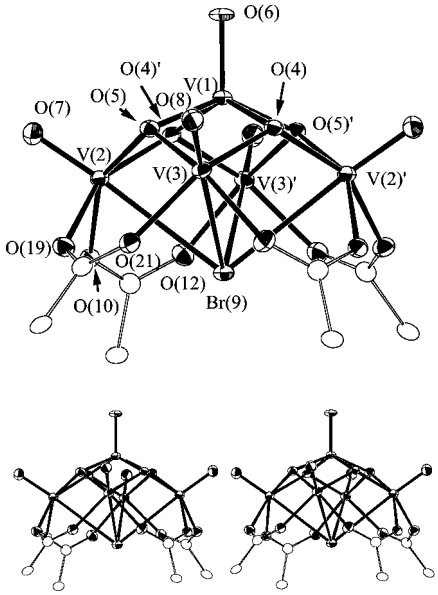

Figure 2. ORTEP representation and stereopair at the 50% probability level of the $[V_5O_9Br(O_2CPh)_4]^{2-}$ anion of **6b**, showing only one C atom of each Ph ring. Primed and unprimed atoms are related by the C_2 axis.

The anion of **4a** consists of a V_5 square pyramid with each vertical face bridged by a μ_3-O^{2-} ion and the basal plane bridged by a μ_4-Cl^- ion. Each basal edge is additionally bridged by a carboxylate group in the familiar *syn,syn* mode, and there is a terminal, multiply-bonded oxygen on each V center (V−O = 1.590(6)-1.603(6) Å). The apical V atom, V(5), which is assigned as the V^V center, is five-coordinate and square-pyramidal, whereas the four basal V^{IV} atoms are distorted octahedral. The V··V separations are of two types, with adjacent basal-basal separations (3.476(3)-3.510(3) Å) significantly longer than basal-apical separations (2.890(3)-2.910(3) Å). The anion has idealized C_{4v} symmetry, none of whose

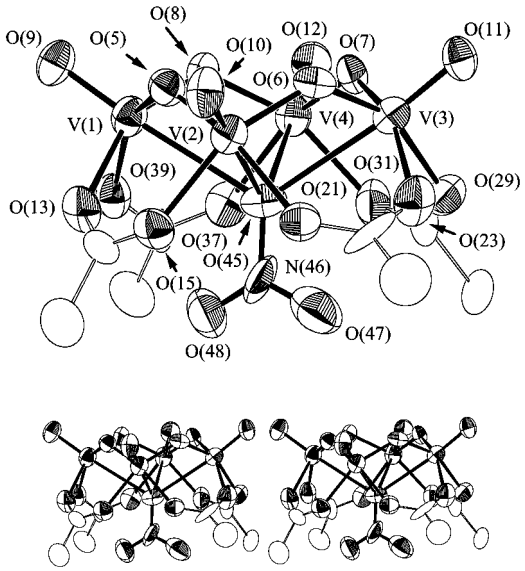

Figure 3. ORTEP representation and stereopair at the 30% probability level of the $[V_4O_8(NO_3)(tca)_4]^{2-}$ anion of **7**, showing only one C atom of the thiophene ring.

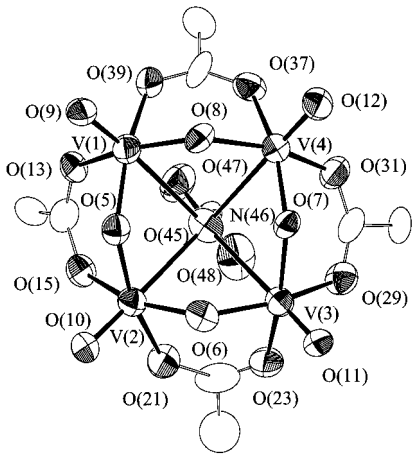

Figure 4. Top view of the $[V_4O_8(NO_3)(tca)_4]^{2-}$ anion of **7** approximately along the virtual C_2 rotation axis showing the orientation of the NO_3^- group.

symmetry elements are crystallographically imposed; the pseudo-C_4 axis passes through V(5) and Cl(6), and a view approximately along this axis is presented in Figure 1 (bottom). (A stereoview is not shown but that for isostructural **6b** is presented in Figure 2 (bottom).) The V−Cl linkages are all remarkably long (2.910(3)-3.165(3) Å), and this feature can reasonably be attributed to a combination of the high Cl coordination number and the *trans* influence of the multiply-bonded $[VO]^{2+}$ unit. Complex **4** provides a very rare example of a tetragonal pyramidal Cl^- ion, i.e. bridging a planar M_4 unit; other examples are the $[Hg_4Cl(C_2B_{10}H_{10})_4]^-$, $[(V_8O_{16})\{V_4O_4(H_2O)_{12}\}(PhPO_3)_8Cl_2]^{2-}$, $[Mn_8O_6Cl_6(O_2CPh)_7(H_2O)_2]$, and $[AgCl_5(L_4)]^-$ (L_4 = a tetradentate ligand) species.[25-27]

The anion of complex **6b** is extremely similar to that of **4a**, except that the Cl^- ion has been replaced by Br^-. The anion now lies on a crystallographic C_2 axis. A comparison of the

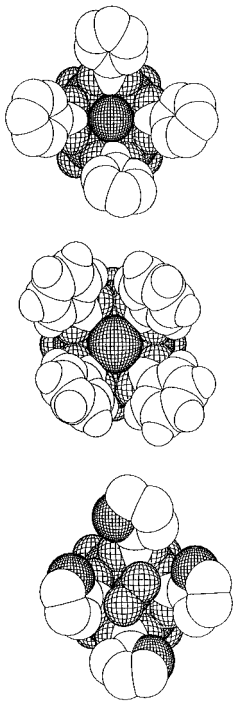

Figure 5. Space-filling representations, viewed approximately along the C_n rotation axes, of the anions of **4a** (top), **6b** (middle), and **7** (bottom).

Table 2. Selected Fractional Coordinates ($\times 10^4$) and Equivalent Isotropic Thermal Parameters[a] (Å^2 × 10) for $(NBzEt_3)_2[V_5O_9Cl(O_2CPh)_4]\cdot MeCN$ (**4a**·MeCN)

atom	*x*	*y*	*z*	B_{eq}
V(1)	1756(1)	5850.8(4)	8712(1)	16
V(2)	562(1)	6110.8(4)	11002(1)	17
V(3)	−1692(1)	5975.4(4)	9803(1)	18
V(4)	−461(1)	5784.3(4)	7456(1)	18
V(5)	14(1)	5496.7(4)	9539(1)	17
Cl(6)	148(2)	6416(1)	8922(2)	20
O(7)	1155(4)	5725(2)	10057(4)	16
O(8)	−569(4)	5797(2)	10604(4)	18
O(9)	−1091(4)	5629(2)	8766(4)	16
O(10)	632(4)	5557(2)	8231(4)	16
O(11)	2601(4)	5537(2)	8601(5)	23
O(12)	841(4)	5947(2)	12133(4)	20
O(13)	−2587(4)	5740(2)	10279(5)	24
O(14)	−783(4)	5448(2)	6650(4)	23
O(15)	−21(4)	5042(2)	9835(4)	23
O(16)	2478(4)	6307(2)	9353(4)	20
C(17)	2349(6)	6522(3)	10153(7)	21
O(18)	1662(4)	6496(2)	10799(4)	21
C(19)	3069(6)	6840(3)	10343(7)	22
O(25)	−269(4)	6571(2)	11441(4)	21
C(26)	−1117(6)	6667(2)	11201(7)	20
O(27)	−1699(4)	6484(2)	10612(5)	22
C(28)	−1525(6)	7047(3)	11652(7)	22
O(34)	−2269(4)	6298(2)	8659(5)	24
C(35)	−2051(6)	6385(2)	7715(8)	27
O(36)	−1435(4)	6211(2)	7161(5)	22
C(37)	−2604(6)	6715(3)	7224(7)	21
O(43)	445(4)	6085(2)	6501(4)	21
C(44)	1335(6)	6178(3)	6543(6)	20
O(45)	1886(4)	6129(2)	7320(4)	21
C(46)	1739(6)	6373(3)	5612(7)	21

[a] $B_{eq} = {}^4/_3\sum\sum \mathbf{B}_{ij}a_ia_j$.

metric parameters of the two anions reveals that the halide identity has an insignificant influence on the structure, except for (i) the longer V−Br distances (average 3.117 Å) compared with V-Cl distances (average 3.001 Å), consistent with the differences in ionic radii (0.15 Å for six coordination), and (ii) the resulting more acute V−Br−V angles (~68.6°) compared

(25) (a) Yang, X.; Knobler, C. B.; Hawthorne, M. F. *Angew. Chem., Int. Ed. Engl.* **1991**, *30*, 1507. (b) Yang, X.; Knobler, C. B.; Zheng, Z.; Hawthorne, M. F. *J. Am. Chem. Soc.* **1994**, *116*, 7142.

(26) (a) Chen, Q.; Zubieta, J. *J. Chem. Soc., Chem. Commun.* **1994**, 1635. (b) Xu, W.; Vittal, J. J.; Puddephatt, R. J. *J. Am. Chem. Soc.* **1995**, *117*, 8362.

(27) Wang, S.; Huffman, J. C.; Folting, K.; Streib, W. E.; Lobkovsky, E. B.; Christou, G. *Angew. Chem., Int. Ed. Engl.* **1991**, *30*, 1672.

Table 3. Selected Fractional Coordinates ($\times 10^4$)[a] and Equivalent Isotropic Thermal Parameters (Å^2 × 10)[b] for $(PPh_4)_2[V_5O_9Br(O_2CPh)_4]$ (**6b**)

atom	*x*	*y*	*z*	B_{eq}
V(1)	10000*	−81(1)	7500*	11
V(2)	9553.9(4)	919.0(5)	6256.0(4)	11
V(3)	8749.2(4)	901.0(5)	7098.2(4)	11
O(4)	9594(2)	334(2)	9725(2)	11
O(5)	9151(2)	348(2)	6676(2)	11
O(6)	10000*	−1137(3)	7500*	15
O(7)	9321(2)	335(2)	5594(2)	15
O(8)	8075(2)	305(2)	6858(2)	16
Br(9)	10000*	2146.6(4)	7500*	11
O(10)	10169(2)	1817(2)	6238(2)	14
C(11)	10795(2)	2100(3)	6680(2)	13
O(12)	11252(2)	1824(2)	7293(2)	14
C(13)	11011(2)	2850(3)	6433(2)	14
O(19)	8809(2)	1893(2)	5822(2)	12
C(20)	8423(2)	2198(3)	5978(2)	14
O(21)	8290(2)	1830(2)	6362(2)	14
C(22)	8106(2)	3093(3)	5715(2)	13

[a] Parameters marked with an asterisk were fixed by symmetry. [b] $B_{eq} = {}^4/_3\sum\sum \mathbf{B}_{ij}a_ia_j$.

Table 4. Selected Fractional Coordinates ($\times 10^4$) and Equivalent Isotropic Thermal Parameters[a] (Å^2 × 10) for $(NEt_4)_2[V_4O_8(NO_3)(tca)_4]\cdot H_2O$ (**7**·H_2O)

atom	*x*	*y*	*z*	B_{eq}
V(1)	1451(1)	8721(1)	2929(3)	69
V(2)	439(2)	9864(1)	2905(3)	69
V(3)	−313(2)	9470(1)	685(3)	64
V(4)	573(2)	8276(1)	843(3)	67
O(5)	1287(6)	9462(5)	2775(9)	70
O(6)	266(6)	9884(4)	1521(8)	62
O(7)	358(7)	8954(5)	273(8)	68
O(8)	1329(6)	8516(5)	1572(9)	67
O(9)	2283(6)	8666(5)	3112(10)	76
O(10)	703(7)	10487(5)	3184(10)	80
O(11)	−409(7)	9852(5)	−301(8)	72
O(12)	946(7)	7940(5)	−89(10)	84
O(13)	1103(7)	8797(5)	4425(10)	73
C(14)	602(11)	9091(8)	4835(18)	80
O(15)	344(8)	9520(6)	4398(9)	82
C(16)	414(14)	8994(8)	5939(14)	87
O(21)	−637(7)	9938(6)	3130(10)	84
C(22)	−1124(12)	9851(8)	2496(20)	85
O(23)	−1137(7)	9725(6)	1547(11)	80
C(24)	−1902(10)	9972(8)	2963(17)	78
O(29)	−1058(8)	8903(6)	397(12)	93
C(30)	−1002(9)	8375(13)	397(18)	102
O(31)	−483(7)	8048(5)	574(11)	80
C(32)	−1573(18)	8078(12)	−64(22)	131(8)
O(37)	466(7)	7642(4)	1941(10)	76
C(38)	725(11)	7603(7)	2867(16)	68
O(39)	1135(7)	7941(4)	3303(10)	78
C(40)	486(13)	7098(8)	3448(15)	85
O(45)	5(7)	8817(5)	2380(10)	78
N(46)	−472(8)	8556(8)	2995(17)	97
O(47)	−321(9)	8323(6)	3764(12)	107
O(48)	−1051(12)	8578(7)	2667(13)	129

[a] $B_{eq} = {}^4/_3\sum\sum \mathbf{B}_{ij}a_ia_j$.

with V−Cl−V angles (∼72°). The anion of **6b** provides a rare example of a tetragonal pyramidal μ_4-Br^- ion, although this coordination geometry does appear more common than for Cl^-, with several previous examples, including $[Ag_4Br_4\{NCH_3(PPh_2)_2\}_2]$, $[Hg_4Br(C_2B_{10}H_{10})_4]^-$, and $(NEt_4)_3(Cu_6Br_9)$.[25,28,29]

The anion of complex **7** is distinctly different from those in **4a** and **6b**, although there are nevertheless some structural relationships. The anion of **7** can be thought of as that of **4a**/**6b** with the apical [VO] unit removed; this converts the V_5 square pyramid into a V_4 square (V··V = 3.267(5)−3.292(5) Å) and the four μ_3-O^{2-} ions into μ-O^{2-} ions. In addition, charge considerations now indicate a V^{IV},$3V^V$ oxidation state description, and the structural parameters in Table 7 indicate four equivalent metal centers, suggesting delocalization of the one d electron between the four metals to give an average oxidation state of +4.75; supporting evidence for this conclusion is presented below.

Table 5. Selected Distances (Å) and Angles (deg) for $[NBzEt_3]_2[V_5O_9Cl(O_2CPh)_4]$ (**4a**)

V(1)·V(2)	3.476(3)	V(2)−O(8)	1.964(6)
V(2)··V(3)	3.509(3)	V(2)−O(25)	2.021(6)
V(3)··V(4)	3.510(3)	V(3)−O(8)	1.959(6)
V(4)··V(1)	3.476(3)	V(3)−O(9)	1.958(5)
V(1)··V(5)	2.899(3)	V(3)−O(13)	1.597(6)
V(2)··V(5)	2.904(3)	V(3)−O(27)	2.015(6)
V(3)··V(5)	2.890(3)	V(3)−O(34)	1.996(6)
V(4)··V(5)	2.910(3)	V(4)−O(9)	1.960(6)
V(1)−Cl(6)	2.956(3)	V(4)−O(10)	1.969(5)
V(2)−Cl(6)	2.910(3)	V(4)−O(14)	1.603(6)
V(3)−Cl(6)	3.165(3)	V(4)−O(36)	2.018(6)
V(4)−Cl(6)	2.972(3)	V(4)−O(43)	2.028(6)
V(1)−O(7)	1.956(6)	V(5)−O(7)	1.884(6)
V(1)−O(10)	1.951(6)	V(5)−O(8)	1.883(6)
V(1)−O(11)	1.590(6)	V(5)−O(9)	1.877(6)
V(1)−O(45)	2.022(6)	V(5)−O(10)	1.889(5)
V(2)−O(7)	1.963(6)	V(5)−O(15)	1.594(6)
Cl(6)−V(1)−O(7)	74.98(17)	Cl(6)−V(1)−O(16)	80.63(19)
Cl(6)−V(1)−O(10)	76.06(19)	Cl(6)−V(1)−O(45)	80.96(18)
Cl(6)−V(1)−O(11)	178.41(22)	O(7)−V(1)−O(10)	79.91(23)
O(7)−V(1)−O(11)	104.21(28)	O(12)−V(2)−O(25)	99.1(3)
O(7)−V(1)−O(16)	91.29(24)	O(18)−V(2)−O(25)	88.01(25)
O(7)−V(1)−O(45)	155.80(23)	Cl(6)−V(3)−O(8)	72.08(22)
O(10)−V(1)−O(11)	102.48(28)	Cl(6)−V(3)−O(9)	72.62(19)
O(10)−V(1)−O(16)	156.50(24)	Cl(6)−V(3)−O(13)	177.33(22)
O(10)−V(1)−O(45)	91.93(23)	Cl(6)−V(3)−O(27)	77.28(19)
O(11)−V(1)−O(16)	100.79(28)	Cl(6)−V(3)−O(34)	78.61(20)
O(11)−V(1)−O(45)	99.77(28)	O(8)−V(3)−O(9)	80.19(23)
O(16)−V(1)−O(45)	87.31(24)	O(8)−V(3)−O(13)	105.29(28)
Cl(6)−V(2)−O(7)	76.04(18)	O(8)−V(3)−O(27)	90.14(25)
Cl(6)−V(2)−O(8)	78.46(17)	O(8)−V(3)−O(34)	150.66(24)
Cl(6)−V(2)−O(12)	177.32(21)	O(9)−V(3)−O(13)	106.7(3)
Cl(6)−V(2)−O(18)	78.53(17)	O(9)−V(3)−O(27)	149.89(24)
Cl(6)−V(2)−O(25)	82.24(18)	O(9)−V(3)−O(34)	90.32(25)
O(7)−V(2)−O(8)	79.18(24)	O(13)−V(3)−O(27)	103.39(28)
O(7)−V(2)−O(12)	102.8(3)	O(13)−V(3)−O(34)	104.0(3)
O(7)−V(2)−O(18)	92.11(24)	O(27)−V(3)−O(34)	84.31(26)
O(7)−V(2)−O(25)	157.79(24)	Cl(6)−V(4)−O(9)	77.47(18)
O(8)−V(2)−O(12)	103.75(26)	Cl(6)−V(4)−O(10)	75.42(19)
O(8)−V(2)−O(18)	156.75(23)	Cl(6)−V(4)−O(14)	179.10(22)
O(8)−V(2)−O(25)	92.12(24)	Cl(6)−V(4)−O(36)	77.74(19)
O(12)−V(2)−O(18)	99.17(27)	Cl(6)−V(4)−O(43)	80.67(19)
O(9)−V(4)−O(10)	78.95(23)	O(10)−V(5)−O(15)	109.17(28)
O(9)−V(4)−O(14)	103.42(27)	V(1)−Cl(6)−V(2)	72.69(7)
O(9)−V(4)−O(36)	93.14(23)	V(1)−Cl(6)−V(4)	71.79(9)
O(9)−V(4)−O(43)	157.69(24)	V(2)−Cl(6)−V(4)	111.95(11)
O(10)−V(4)−O(14)	104.9(3)	V(1)−Cl(6)−V(3)	109.42(10)
O(10)−V(4)−O(36)	153.07(24)	V(2)−Cl(6)−V(3)	70.44(7)
O(10)−V(4)−O(43)	91.34(24)	V(3)−Cl(6)−V(4)	69.70(9)
O(14)−V(4)−O(36)	102.0(3)	V(1)−O(7)−V(2)	125.0(3)
O(14)−V(4)−O(43)	98.45(28)	V(1)−O(7)−V(5)	98.03(25)
O(36)−V(4)−O(43)	86.49(25)	V(2)−O(7)−V(5)	98.02(25)
O(7)−V(5)−O(8)	83.27(25)	V(2)−O(8)−V(3)	126.9(3)
O(7)−V(5)−O(9)	140.46(25)	V(2)−O(8)−V(5)	98.02(25)
O(7)−V(5)−O(10)	83.36(25)	V(3)−O(8)−V(5)	97.53(25)
O(7)−V(5)−O(15)	110.0(3)	V(3)−O(9)−V(4)	127.3(3)
O(8)−V(5)−O(9)	84.26(24)	V(3)−O(9)−V(5)	97.78(24)
O(8)−V(5)−O(10)	140.82(26)	V(4)−O(9)−V(5)	98.62(25)
O(8)−V(5)−O(15)	110.0(3)	V(1)−O(10)−V(4)	124.9(3)
O(9)−V(5)−O(10)	83.07(25)	V(1)−O(10)−V(5)	98.01(25)
O(9)−V(5)−O(15)	109.5(3)	V(4)−O(10)−V(5)	97.91(25)

(28) Schubert, U.; Neugebauer, D.; Aly, A. A. M. *Z. Anorg. Allg. Chem.* **1980**, *464*, 217.
(29) Andersson, S.; Jagner, S. *Acta Chem. Scand.* **1989**, *43*, 39.

Table 6. Selected Distances (Å) and Angles (deg) for **6b**

Br(9)−V(2)	3.110(1)	V(2)−O(5)	1.960(3)
Br(9)−V(3)	3.125(1)	V(2)−O(7)	1.596(3)
V(1)−V(2)	2.915(1)	V(2)−O(10)	2.013(3)
V(1)−V(3)	2.899(1)	V(2)−O(19)	2.034(3)
V(2)−V(3)	3.519(1)	V(3)−O(4)	1.957(3)
V(2)−V(3)′	3.513(1)	V(3)−O(5)	1.952(3)
V(1)−O(4)	1.885(3)	V(3)−O(8)	1.602(3)
V(1)−O(5)	1.875(3)	V(3)−O(12)′	2.029(3)
V(1)−O(6)	1.607(4)	V(3)−O(21)	1.989(3)
V(2)−O(4)′	1.969(3)		
V(2)−Br(9)−V(2)′	106.20(4)	O(5)−V(1)−O(6)	110.34(9)
V(2)−Br(9)−V(3)	68.715(22)	Br(9)−V(2)−O(4)′	76.85(9)
V(2)−Br(9)−V(3)′	68.583(23)	Br(9)−V(2)−O(5)	76.07(9)
V(3)−Br(9)−V(3)′	105.34(4)	Br(9)−V(2)−O(7)	176.88(12)
O(4)−V(1)−O(4)′	140.92(18)	Br(9)−V(2)−O(10)	77.72(9)
O(4)−V(1)−O(5)	83.45(13)	Br(9)−V(2)−O(19)	74.62(9)
O(4)′−V(1)−O(5)	83.19(13)	O(4)′−V(2)−O(5)	78.91(12)
O(4)−V(1)−O(6)	109.54(9)	O(4)′−V(2)−O(7)	105.25(14)
O(5)−V(1)−O(5)′	139.31(18)	O(4)′−V(2)−O(10)	90.95(13)
O(4)′−V(2)−O(19)	151.43(13)	O(4)−V(3)−O(12)′	91.31(13)
O(5)−V(2)−O(7)	106.51(14)	O(4)−V(3)−O(21)	151.65(13)
O(5)−V(2)−O(10)	153.42(13)	O(5)−V(3)−O(8)	105.07(14)
O(5)−V(2)−O(19)	92.73(12)	O(5)−V(3)−O(12)′	152.58(13)
O(7)−V(2)−O(10)	99.83(15)	O(5)−V(3)−O(21)	91.11(13)
O(7)−V(2)−O(19)	103.32(14)	O(8)−V(3)−O(12)′	102.32(14)
O(10)−V(2)−O(19)	84.51(12)	O(8)−V(3)−O(21)	101.46(15)
Br(9)−V(3)−O(4)	76.61(9)	O(12)′−V(3)−O(21)	84.73(13)
Br(9)−V(3)−O(5)	75.78(9)	V(1)−O(4)−V(2)′	98.26(13)
Br(9)−V(3)−O(8)	176.56(12)	V(1)−O(4)−V(3)	97.93(14)
Br(9)−V(3)−O(12)′	76.96(9)	V(2)′−O(4)−V(3)	126.95(15)
Br(9)−V(3)−O(21)	75.14(9)	V(1)−O(5)−V(2)	98.93(13)
O(4)−V(3)−O(5)	79.61(13)	V(1)−O(5)−V(3)	98.45(14)
O(4)−V(3)−O(8)	106.80(14)	V(2)−O(5)−V(3)	128.15(15)

Table 7. Selected Distances (Å) and Angles (deg) for $[NEt_4]_2[V_4O_8(NO_3)(tca)_4]$ (**7**)

V(1)−O(5)	1.783(12)	V(4)−O(8)	1.780(12)
V(1)−O(8)	1.808(11)	V(4)−O(12)	1.586(12)
V(1)−O(9)	1.572(12)	V(4)−O(31)	2.068(13)
V(1)−O(13)	2.020(13)	V(4)−O(37)	2.055(12)
V(1)−O(39)	1.988(11)	O(45)−N(46)	1.335(20)
V(2)−O(5)	1.851(12)	O(47)−N(46)	1.157(20)
V(2)−O(6)	1.792(11)	O(48)−N(46)	1.158(21)
V(2)−O(10)	1.590(12)	V(1)−O(45)	2.79(1)
V(2)−O(15)	2.073(13)	V(2)−O(45)	2.67(1)
V(2)−O(21)	2.034(14)	V(3)−O(45)	2.71(1)
V(3)−O(6)	1.803(11)	V(4)−O(45)	2.56(1)
V(3)−O(7)	1.821(13)	V(1)··V(2)	3.287(5)
V(3)−O(11)	1.555(11)	V(1)··V(4)	3.292(5)
V(3)−O(23)	1.981(14)	V(2)··V(3)	3.287(5)
V(3)−O(29)	1.961(14)	V(3)··V(4)	3.267(5)
V(4)−O(7)	1.799(12)		
O(45)−N(46)−O(47)	123.5(17)	V(1)−O(45)−V(2)	73.8(3)
O(45)−N(46)−O(48)	112.9(21)	O(47)−N(46)−O(48)	123.6(23)
V(1)−V(2)−V(3)	91.2(1)	V(2)−V(1)−V(4)	88.1(1)
V(2)−V(3)−V(4)	88.5(1)	V(1)−O(45)−V(4)	75.7(4)
V(2)−O(45)−V(3)	75.1(3)	V(3)−O(45)−V(4)	76.4(3)

The final main difference between the anions of **7** and **4a**/**6b** is the presence of a μ_4-NO_3^- ion rather than a halide. The former bridges the four V ions using only one of its oxygen atoms, O(45). This μ_4,η^1 mode is extremely rare for NO_3^-; complex **7** was the first example, and the one-electron oxidized version, $[V_4O_8(NO_3)(O_2CR)_4]^-$, has since been reported by others.[21] The V−O(45) distances are all long (2.56(1)−2.79(1) Å). The anion has no crystallographic symmetry, but approximates C_{4v}, or C_{2v} if the orientation of the NO_3^- group is taken into account, as emphasized in the top view along the pseudo-C_4 (C_2) axis in Figure 4.

It is interesting to note that the $[V_4O_8X(O_2CR)_4]^z$ (X = NO_3; z = −1 or −2) structure in **7** and $[V_4O_8(NO_3)(O_2CMe)_4]^-$ exists with X = K^+ and $z = +1$ in $[KV_4O_8(O_2CCH_2Bu^t)_4]^+$ (i.e. $4V^V$); the K^+ ion is very approximately in the position occupied by O(45) in Figure 3, where it is held by interactions with the carboxylate oxygen atoms (average K−O = 3.15(1) Å; average K··V = 2.825(5) Å).[16] It is thus of interest to realize that this cavity between the carboxylate groups on the square face of $[V_4O_8X(O_2CR)_4]^z$ or the basal face of $[V_5O_9X(O_2CR)_4]^{2-}$ can accommodate either anionic or cationic X groups and is currently known with X = Cl^-, Br^-, NO_3^-, and K^+. A space-filling representation of the anions in this cavity for **4a**, **6b**, and **7** is shown in Figure 4.

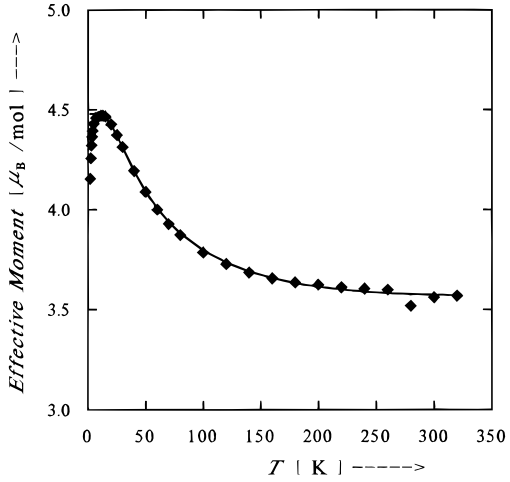

Figure 6. Plot of effective magnetic moment (μ_{eff}) per V_5 anion *vs* temperature for complex **4b**. The solid line is a fit of the data to the appropriate theoretical expression; see the text for the fitting parameters.

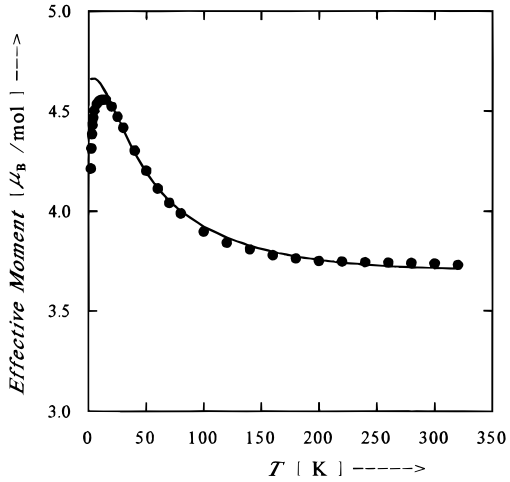

Figure 7. Plot of effective magnetic moment (μ_{eff}) per V_5 anion *vs* temperature for complex **6a**. The solid line is a fit of the data to the appropriate theoretical expression; see the text for the fitting parameters.

Magnetochemical Studies. Variable-temperature magnetic susceptibility data were collected on powdered samples of complexes **4b** , **6a**·MeCN·H_2O and **7** in the range 2.00−320 K in a 10 kG applied field. For complex **4b**, the effective magnetic moment, μ_{eff} per V_5, slowly increases from 3.57 μ_B at 320 K to a maximum of 4.47 μ_B at 11.0 K and then decreases slightly to 4.15 μ_B at 2.00 K. These correspond to $\chi_M T$ values of 1.59, 2.50, and 2.15 cm^3 K mol^{-1}, respectively. For complex **6a**, the same μ_{eff} *vs T* profile is observed with corresponding values of 3.73, 4.56, and 4.21 μ_B at 320, 11.0 and 2.00K, respectively. These data for **4b** and **6a** are plotted in Figures 6 and 7.

From a magnetochemical viewpoint, **4b** and **6a** are effectively tetranuclear because only the four V^{IV} centers possess unpaired electrons. For such a "tetranuclear" complex comprising four non-interacting V^{IV} ($S = {}^1/_2$) centers, the spin-only ($g = 2.00$)

μ_{eff} and $\chi_M T$ values (per V_4) would be 3.46 μ_B and 1.50 cm^3 K mol^{-1}, respectively. The experimental μ_{eff} and $\chi_M T$ values are thus indicative of the presence of exchange interactions that are ferromagnetic in nature; indeed, the values at 11.0 K may be compared with the spin-only values of 4.90 μ_B and 3.00 cm^3 K mol^{-1} expected for a S = 2 state. The μ_{eff} *vs T* profile in Figure 6 is also similar to those seen for ferromagnetically-coupled $S = {}^1/_2$/S $= {}^1/_2$ dinuclear species, for example [CuVO(fsa)$_2$en]·MeOH (fsa = a polydentate Schiff base ligand).[30]

In order to fit the experimental data, a model was derived based on the essentially C_{4v} symmetry seen in the structures of **4a** and **6b**, i.e. a square V_4 unit. This model is shown here

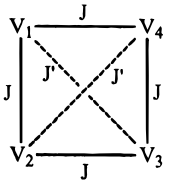

employing the metal numbering scheme of Figure 1 and requires two exchange parameters, *J* and *J*′, to gauge all possible pairwise exchange interactions: $J = J_{cis}$, the interaction between adjacent V^{IV} centers bridged by both μ_3-O^{2-} and μ_4-X^- (X = Cl, Br) ions, and $J' = J_{trans}$, the interaction across the diagonal of the V_4 square, which is mediated by only the μ_4-X^- ion (the coupling *via* the apical, diamagnetic V^V being assumed to be zero). The Heisenberg spin Hamiltonian for this system is given by eq 1: this can be converted into an equivalent form (eq 2)

$$\hat{H} = -2J(\hat{S}_1\cdot\hat{S}_2 + \hat{S}_2\cdot\hat{S}_3 + \hat{S}_3\cdot\hat{S}_4 + \hat{S}_1\cdot\hat{S}_4) - 2J'(\hat{S}_1\cdot\hat{S}_3 + \hat{S}_2\cdot\hat{S}_4) \quad (1)$$

by using the Kambe vector coupling method and the definitions

$$\hat{H} = -J(\hat{S}_T{}^2 - \hat{S}_A{}^2 - \hat{S}_B{}^2) - J'(\hat{S}_A{}^2 + \hat{S}_B{}^2 - \hat{S}_1{}^2 - \hat{S}_2{}^2 - \hat{S}_3{}^2 - \hat{S}_4{}^2) \quad (2)$$

$\hat{S}_A = \hat{S}_1 + \hat{S}_3$, $\hat{S}_B = \hat{S}_2 + \hat{S}_4$, and $\hat{S}_T = \hat{S}_A + \hat{S}_B$, where S_T is the total spin for the complete V_4 unit. The eigenvalues of the spin Hamiltonian in eq 2 are given by eq 3, where $E(S_T)$ is the energy

$$E(S_T) = -J[S_T(S_T + 1) - S_A(S_A + 1) - S_B(S_B + 1)] - J'[S_A(S_A + 1) + S_B(S_B + 1)] \quad (3)$$

of state S_T; the $S_i(S_i + 1)$ ($i = 1, 2, 3, 4$) terms contribute equally to all S_T states and have been ignored. There are a total of six S_T states (two $S_T = 0$, three $S_T = 1$, and one $S_T = 2$). The S_T and corresponding $E(S_T)$ terms were incorporated into the Van Vleck equation to provide a theoretical χ_M *vs T* expression, and this was employed to least-squares-fit the experimental χ_M *vs T* data for **4b** and **6a**. The solid lines in Figures 6 and 7 show the results of these fits: the fitting parameters in the format **4b**/**6a** are $J = +39.7/+46.4$ cm^{-1}, $J' = -11.1/-18.2$ cm^{-1}, and $g = 1.83/1.90$, with temperature independent paramagnetism (TIP) held constant at 500×10^{-6} cm^3 mol^{-1}, and no paramagnetic impurity correction being included. These fits indicate that **4b** and **6a** have a $S_T = 2$ ground state arising from $S_A = 1$ and $S_B = 1$, i.e. (2,1,1) in the format (S_T,S_A,S_B). The excited states in order of increasing energy are (0,0,0), (1,0,1), (1,1,0), (1,1,1), and (0,1,1) at energies above the ground state of 35.0/19.9, 57.2/92.9, 57.2/92.9, 158.9/185.8, and 238.3/278.7 cm^{-1}, respectively, for **4b**/**6a**.

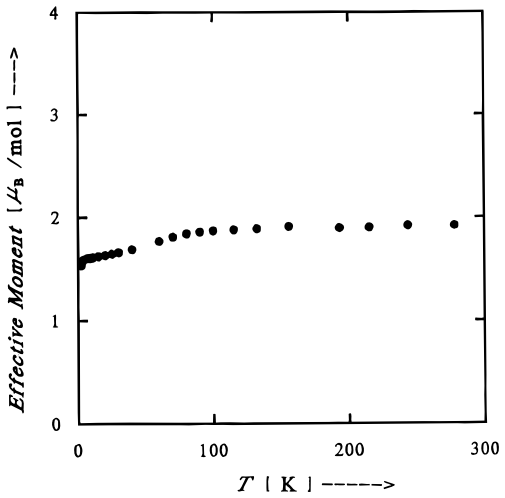

Figure 8. Plot of effective magnetic moment per V_4 anion *vs* temperature for complex **7**.

For both fits, there is a divergence between the calculated behaviors (solid lines in Figures 6 and 7) and the experimental points at low temperatures: for **4b**, the calculated behavior is a plateau between 11.0 and 2.00 K, whereas the experimental μ_{eff} values decrease below 11.0 K. Such low temperature decreases in μ_{eff} values are due in general to a number of reasons, primarily zero field splitting (ZFS) of a $S \geq 1$ ground state, and *inter*molecular exchange interactions that are weakly antiferromagnetic in nature. For **6b**, the low temperature divergence is more marked, becoming evident at ≤15.0 K. Further discussion of this matter requires a better assessment of the magnitude of ZFS in these complexes, which is addressed below (*vide infra*).

For complex **7**, μ_{eff} per V_4 is essentially temperature-independent at temperatures ≥70 K, decreasing only slightly from 1.92 μ_B at 278 K to 1.81 μ_B at 70 K, and then decreases slightly more rapidly to 1.53 μ_B at 2.2 K. These data are shown in Figure 8. The μ_{eff} value and its near temperature-independence are consistent with a $S = {}^1/_2$ cluster, as expected for the V^{IV},3V^V oxidation state description deduced from the crystal structure, and provide independent support for this earlier conclusion.

Magnetization *vs* Magnetic Field Studies. In order to further probe the nature of the ground states of **4b** and **6a**, magnetization (*M*) *vs* field (*H*) studies were performed in temperature and field ranges of 2.00−30.0 K and 0.500−50.0 kG, respectively. The results are shown in Figures 9 and 10, plotted as reduced magnetization ($M/N\mu_B$) *vs* H/T, where *N* is Avogadro's number and μ_B is the Bohr magneton. For complexes with $S_T = 2$ ground states that exhibit no ZFS, the $M/N\mu_B$ *vs* H/T plots should saturate at $M/N\mu_B$ values of gS_T (i.e. 4 for $g = 2.0$ and $S_T = 2$), and the various isofield lines should be superimposed. As can be seen in Figures 9 and 10, at the highest H/T value accessible ($T = 2.00$ K, $H = 50$ kG), the $M/N\mu_B$ values are 3.41 and 3.54, respectively, with the plots not quite having reached saturation. In addition, the various isofield lines are superimposed, suggesting small ZFS. The data were fit to a model that assumes that only the ground state is populated and which includes axial ZFS ($D\hat{S}_z{}^2$) and the Zeeman interaction; a matrix diagonalization procedure described elsewhere was employed.[31] The fits are shown as solid lines in

(30) (a) Kahn, O.; Galy, J.; Tola, P.; Coudanne, H. *J. Am. Chem. Soc.* **1978**, *100*, 3931. (b) Kahn, O.; Galy, J.; Journaux, Y.; Saud, J.; Morganstern-Badarau, I. *J. Am. Chem. Soc.* **1982**, *104*, 2165.

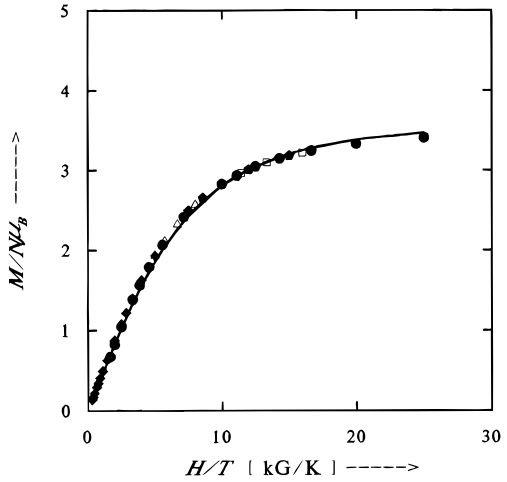

Figure 9. Plot of reduced magnetization ($M/N\mu_B$) *vs* H/T for complex **4b** at magnetic field (H) values of 10 (◆), 20 (△), 30 (▲), 40 (□), and 50 kG (●). The solid lines are fits to the appropriate theoretical equation; see the text for the fitting parameters.

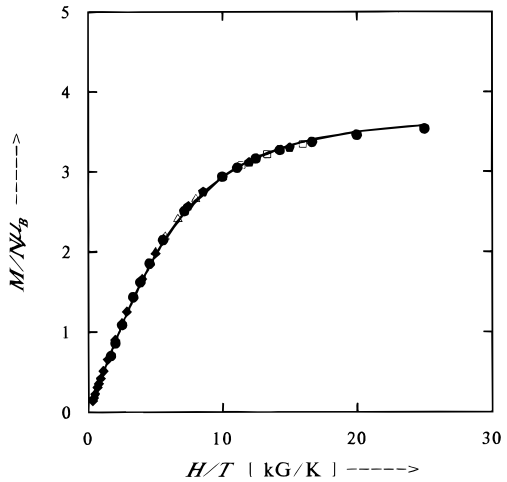

Figure 10. Plot of reduced magnetization ($M/N\mu_B$) *vs* H/T for complex **6a** at magnetic field (H) values of 10 (◆), 20 (△), 30 (▲), 40 (□), and 50 kG (●). The solid lines are fits to the appropriate theoretical equation; see the text for the fitting parameters.

Figures 9 and 10; the fitting parameters are $S_T = 2$ and $D = 0.00$ cm^{-1} for both complexes, where D is the axial ZFS parameter, and $g = 1.80$ and 1.90 for **4b** and **6a**, respectively.

The confirmation of $S_T = 2$ ground states and no ZFS allows the low temperature divergence between calculated and experimental μ_{eff} values in Figures 6 and 7 to be assigned as most likely arising from weak, intermolecular antiferromagnetic exchange interactions. Further, presence of solvent (MeCN, H_2O) in the formulation of complex **6a** suggests that the H_2O may be hydrogen-bonding with and bridging between carboxylate groups on two different anions, providing stronger intermolecular interactions, and a greater resultant divergence at low temperatures, than in **4b**, which analyzes as solvent-free.

Origin of the $S_T = 2$ Ground State. Many monoatomically-bridged dinuclear V^{IV} complexes are known for which magnetochemical studies have been performed, and the exchange interactions are almost always antiferromagnetic in nature (J negative) leading to $S_T = 0$ ground states.[24,32] Exceptions include: $[VO(salpn)]_n$ (salpn = *N*,*N*′-propylenebis(salicylaldiminate), which is a one-dimensional chain propagated by intermolecular ···V=O···V=O··· interactions and has an exchange interaction between adjacent V^{IV} centers of $J = +4.1$ cm^{-1} (rationalized as due to the d_{xy} magnetic orbitals all being perpendicular to the chain axis and thus orthogonal);[33] and $[VO(Hsabhea)]_2$ and a related complex (H_3sabhea = *N*-salicylidene-2-(bis(2-hydroxyethyl)amino)ethylamine) which contain alkoxide-bridged bis(vanadyl) units and have J values of $+3.1$ and $+10.6$ cm^{-1}.[34] It is of importance, therefore, to rationalize the unusual and relatively strong ferromagnetic (J) interactions between adjacent V^{IV} centers in **4b** and **6a**, which dominate the weaker antiferromagnetic (J') interactions and yield the $S_T = 2$ ground state. The relatively large magnitude of J ($\sim$40 cm^{-1}) is not itself unusual for V^{IV} in *hetero*metallic complexes: in several $[Cu^{II}_nVO]$ ($n = 1,2$) systems, strong ferromagnetic interactions have been found between Cu^{II} and V^{IV} by both Kahn[30,35] and Gatteschi;[36] for example, J is $+59$ cm^{-1} for $[CuVO(fsa)_2en]\cdot MeOH$.[30,35] Ferromagnetic coupling in this and related systems is linked to strict orthogonality between the Cu^{II} $d_{x^2-y^2}$ and VO d_{xy} magnetic orbitals, which are of σ and π symmetry, respectively, *vis-à-vis* the ligand bonding framework.

The case of a polynuclear V system such as $[V_5O_9X(O_2CR)_4]^{2-}$ (X = Cl, Br) is more complicated owing to the homometallic character of the system and the essentially symmetry-equivalent nature of the four paramagnetic V^{IV} centers. Taking the VO multiple bond as the z axis and the V−O (carboxylate) bonds as the x and y axes, then the local symmetry at each V^{IV} is C_{4v} and the magnetic orbital is d_{xy}; the four magnetic orbitals are thus part of the π network. Because of the orientation of the four d_{xy} orbitals, the exchange interaction between adjacent V^{IV} centers may arise from direct overlap of d_{xy} orbitals, a superexchange mechanism involving bridging ligand filled orbitals, or both. The direct overlap mechanism is unlikely to be a major contributor in this case: the large $V^{IV}\cdot\cdot V^{IV}$ separations ($\sim$3.5 Å) and relative disposition of d_{xy} magnetic orbitals appear to allow, at best, only very small overlap between the latter. In any case, direct overlap of magnetic orbitals normally results in antiferromagnetic exchange interactions,[37] except in the case of accidental orthogonality due to certain angles between the magnetic orbitals involved; while commonly found in Cu^{II}_2 systems, such a situation is unlikely to arise in the present complexes.[37] It does not therefore appear that direct overlap can provide an explanation for the ferromagnetic interactions in **4b** and **6a**.

In contrast to the above, considerations of superexchange pathways provide a rationalization of the observed behavior.

(31) Hendrickson, D. N.; Christou, G.; Schmitt, E. A.; Libby, E.; Bashkin, J. S.; Wang, S.; Tsai, H.-L.; Vincent, J. B.; Boyd, P. D. W.; Huffman, J. C.; Folting, K.; Li, Q.; Streib, W. E. *J. Am. Chem. Soc.* **1992**, *114*, 2455.

(32) For example, see: (a) Wieghardt, K.; Bossek, U.; Volckmar, K.; Swiridoff, W.; Weiss, J. *Inorg. Chem.* **1984**, *23*, 1387. (b) Toftlund, H.; Larsen, S.; Murray, K. S. *Inorg. Chem.* **1991**, *30*, 3964. (c) Collison, D.; Eardley, D. R.; Mabbs, F. E.; Powell, A. K.; Turner, S. S. *Inorg. Chem.* **1993**, *32*, 664. (d) Neves, A.; Wieghardt, K.; Nuber, B.; Weiss, J. *Inorg. Chim. Acta* **1988**, *150*, 183. (e) Das, R.; Nanda, K. K.; Mukherjee, A. K.; Mukherjee, M.; Helliwell, M.; Nag, K. *J. Chem. Soc., Dalton Trans.* **1993**, 2241. (f) Carrano, C. J.; Nunn, C. M.; Quan, R.; Bonadies, J. A.; Pecoraro, V. L. *Inorg. Chem.* **1990**, *29*, 944. (g) Kitagawa, S.; Munakata, M.; Ueda, M.; Yonezawa, T. *Inorg. Chim. Acta* **1990**, *175*, 3. (h) Priebsch, W.; Weidemann, C.; Rehder, D.; Kopf, J. *Z. Naturforsch.* **1986**, *41b*, 834.

(33) Drake, R. F.; Crawford, V. H.; Hatfield, W. E.; Simpson, G. D.; Carlisle, G. O. *J. Inorg. Nucl. Chem.* **1975**, *37*, 291.

(34) Plass, W. *Angew. Chem., Int. Ed. Engl.* **1996**, *35*, 627.

(35) (a) DeLoth, P.; Karafiloglou, P.; Daudey, J. P.; Kahn, O. *J. Am. Chem. Soc.* **1988**, *110*, 5676. (b) Julve, M.; Verdaguer, M.; Charlot, M. F.; Kahn, O.; Claude, R. *Inorg. Chim. Acta* **1984**, *82*, 5.

(36) Bencini, A.; Benelli, C.; Dei, A.; Gatteschi, D. *Inorg. Chem.* **1985**, *24*, 695.

(37) Kahn, O. *Molecular Magnetism*, VCH: Weinheim, Germany, 1993.

Consider first a V^{IV}_2 unit bridged by a μ_2-O^{2-} ion, such as the V(1)−O(7)−V(2) fragment in Figure 1.

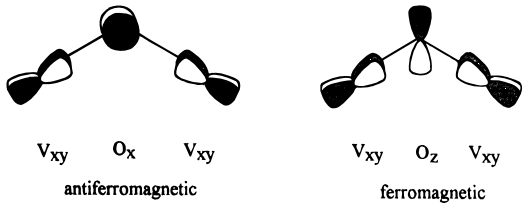

Overlap of the vanadium d_{xy} magnetic orbitals with the O p_π orbitals would be expected to give an overall antiferromagnetic interaction: nonzero net overlap between d_{xy} and oxygen p_x orbitals would provide a strong antiferromagnetic contribution to J which would dominate the ferromagnetic contribution arising from the orthogonality (zero net overlap) of d_{xy} and oxygen p_z orbitals. Dinuclear V^{IV}_2 complexes with a single, bent O^{2-}-bridge are not known, but the same kind of overlap in a V^{IV}_2 complex with a linear O^{2-} bridge gives a strongly antiferromagnetically coupled system, diamagnetic even at room temperature.[32b]

If a $[V^{IV}_4(\mu\text{-}O)_4]$ square is now considered, the same overlap considerations predict a strongly antiferromagnetically-coupled system. So why are **4b** and **6a** ferromagnetic? The answer, we believe, is that they contain a V^V capping the V_4 square by attachment to the four bridging O^{2-} ions; this strongly stabilizes the oxygen p_x orbitals (which point towards the V^V ion), greatly increasing the energy mismatch between them and the vanadium d_{xy} orbitals and effectively shutting down this exchange pathway. This leaves the pathway involving the oxygen p_z orbital as the major contributor to the overall J, which is thus ferromagnetic. In essence, the single lone pair on the μ_3-O^{2-} ions available to mediate magnetic exchange between V^{IV} centers is orthogonal to the magnetic orbitals, and J is therefore ferromagnetic. Note that overlap of the V d_{xy} orbitals with the RCO_2^- π system would be non-zero but undoubtedly relatively weak, providing an antiferromagnetic contribution to J of probably only zero to -3 cm^{-1}. The above analysis predicts that the hypothetical complex $[V_4O_8X(O_2CR)_4]^{4-}$, structurally analogous to **7** but at the $4V^{IV}$ oxidation level, should have J negative and thus an $S_T = 0$ ground state. Such a molecule is not available to test this prediction.

The antiferromagnetic J' ($=J_{trans}$) interaction is less easily rationalized, although the large internuclear separation would appear to totally rule out any possibility of direct overlap of V d_{xy} orbitals. A superexchange pathway involving the μ_4-X^- (X = Cl, Br) ion would appear the most likely possibility, and the following is suggested, involving the X p_x or p_y orbital:

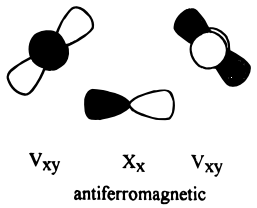

It is perhaps pertinent to note that Br-for-Cl substitution (i.e., **6a** *vs* **4b**) causes only a 17% change in J but a 64% change in J', suggesting J' is the more sensitive to the identity of X, consistent with the proposed pathway in which the larger Br orbitals would provide better overlap. More data are required, however, before any such relationship can be more securely tested.

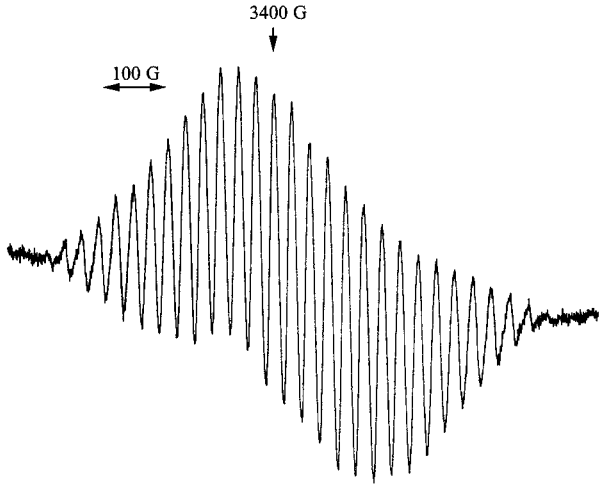

Figure 11. X-band EPR spectrum at ~25 °C of a toluene−MeCN (1:2) solution of $(NEt_4)_2[V_4O_8(NO_3)(tca)_4]$ (**7**).

EPR Spectroscopy. The conclusion from the crystal structure and magnetic studies on **7** that this complex has a $V^{IV},3V^V$ oxidation state ($S = {}^1/_2$) suggested that it should be EPR-active and that this technique might shed light on the degree of delocalization of the single unpaired electron. Thus, the EPR spectrum of **7** was recorded in a toluene−MeCN (1:2) solution at room temperature (~25 °C) and is shown in Figure 11. The spectrum shows a signal at $g \sim 2$, exhibiting an isotropic 29-line hyperfine pattern with the two weakest, outermost lines barely discernible above background noise. This 29-line signal can be readily assigned to hyperfine interactions between the unpaired electron and four equivalent V nuclei ($I = {}^7/_2$, ~100% natural abundance). This supports the conclusion from the crystal structure data that the four V atoms are equivalent, indicating delocalization of the unpaired electron over the four V centers to give each a formal oxidation state of +4.75. Analysis of the EPR signal and its hyperfine structure, and correcting for second-order effects, gave $g = 1.97$ and $A = 28.6$ G. Note also that (i) the 29-line EPR signal supports retention of the tetranuclear nature of **7** on dissolution in MeCN, and (ii) the solid-state structure of **7** approximates to C_{2v} because of the orientation of the NO_3^- group, but it is reasonable that in solution this group is fluxional *via* rotation about the O(45)−N(46) bond to give effective C_{4v} solution symmetry, consistent with the EPR spectrum.

When the solution is cooled, the EPR signal progressively broadens and the hyperfine structure is lost, preventing any conclusions being drawn concerning the possibility of localization of the electron on a single V atom. The complexes $[V_2W_{16}P_2O_{62}]^{9-}$ and $[V_3W_{15}P_2O_{62}]^{10-}$ contain V^{IV},V^V and $V^{IV},2V^V$, respectively, and exhibit similar delocalization of a single electron over their multiple V atoms at room temperature: the solution EPR spectra of the former and latter show 15-line and 22-line hyperfine patterns, respectively.[38] Below 100 K, however, the electron delocalization (hopping or detrapping) is slow on the EPR time scale for both polyoxometallates, and the spectra are characteristic of mononuclear V^{IV} species.

^{1}H NMR Spectroscopy. The NMR spectra of complexes **4b**, **5**, and **6a** in CD_3CN have been recorded to probe the nature of these $[V_5O_9X]$ species in solution. Spectra were recorded at a number of temperatures in the −40 to +50 °C range, and selected data are presented in Table 8. The spectrum for **6a** at ~23 °C is presented in Figure 12. In addition to NEt_4^+, lattice

(38) Harmalker, S. P.; Leparulo, M. A.; Pope, M. T. *J. Am. Chem. Soc.* **1983**, *105*, 4286.

Table 8. ^{1}H NMR Isotropic Shifts[a] at Selected Temperatures for Complexes **4b**, **5**, and **6a**

complex	*T*, °C[b]	*o*[c]	*m*[d]	*p*[d]
4b	50	−1.7	0.21	−2.31
	23	−1.8	0.25	−2.59
	−42	∼−2.5	0.37	−3.76
5	50	−1.8	0.32	(2.76)
	22	−2.1	0.39	(3.16)
	−38	−3.0	0.53	(4.45)
6a	50	−1.7	0.24	−2.36
	23	−1.9	0.30	−2.66
	−41	−2.7	0.48	−3.93

[a] ppm, CD_3CN solution; referenced to NH_4O_2CPh (o = 7.59, m/p = 7.52 ppm) for **4b** and **6a**, and $HO_2CC_6H_4$-*p*-Me (o = 7.99, m = 7.20, *p*-Me = 2.40 ppm) for **5**. [b] ±1 °C. [c] ±0.1 ppm. [d] ±0.03 ppm; numbers in parentheses are for Me groups at that position.

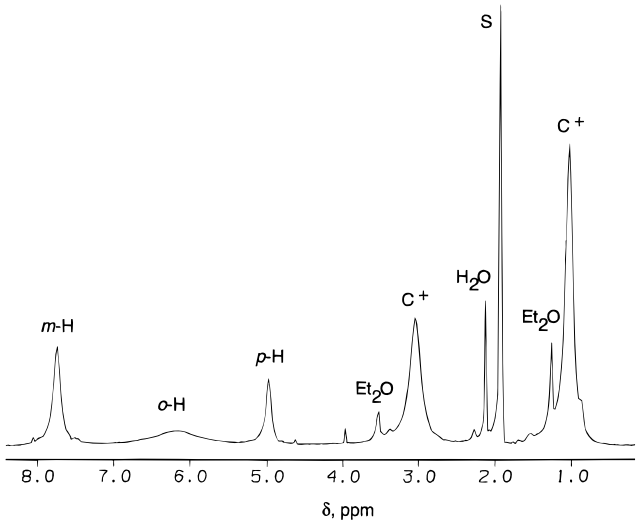

Figure 12. 300 MHz ^{1}H NMR spectrum at ∼23 °C for $(NEt_4)_2[V_5O_9Br(O_2CPh)_4)]$ (**6a**). s = solvent protio signal, $C^+ = NEt_4^+$.

solvent, and H_2O impurity peaks, there are three paramagnetically-shifted and broadened resonances in the δ = 5−8 ppm region assignable to the benzoate hydrogen atoms of the anion; individual assignments were made by considerations of relative integration ratios (approximately 2:2:1) and relative peak linewidths, the *o*-hydrogen being the most broadened owing to its closest separation from the paramagnetic V centers (r^{-6} dependence). When expressed as isotropic shift (displacement from the resonance position in an analogous diamagnetic complex or, more conveniently, the free ligand value), the *o*- and *p*-hydrogen isotropic shifts are negative (upfield) while that for the *m*-hydrogen is positive (downfield). This alternating upfield−downfield−upfield isotropic shift pattern for a phenyl ring is the usual signature of contact shifts *via* a π spin delocalization mechanism. The same spectral pattern and very similar isotropic shifts are observed for the corresponding Cl^- complex **4b** (Table 8). A single set of $PhCO_2^-$ resonances is consistent with effective C_{4v} symmetry for the anions in solution and thus the retention of their tetranuclear nature in MeCN.

As discussed in the previous section, the vanadium d_{xy} magnetic orbitals are part of the π network and have net overlap with the RCO_2^- π-system. This overlap will result in parallel spin at the V atoms being directly delocalized into the $-CO_2$ π-system and then onto the Ph ring to give parallel spin density at *o*- and *p*-C positions; this in turn will lead *via* spin polarization effects to antiparallel spin at the *o*- and *p*-hydrogen atoms and resulting upfield shifts. Similar spin polarization effects give parallel spin density at the *m*-hydrogen atoms and resulting downfield shifts.[39] In an absolute sense, the isotropic shifts of the benzoate hydrogen resonances are small, consistent with free rotation about the C−C bond, which decreases the influence of the π-spin delocalization mechanism.

The presence of a π-spin delocalization mechanism is supported by the spectrum of **5**; substitution of a Me group at the benzoate *para* position causes the *p*-Me isotropic shift to now be positive (i.e., downfield of its "diamagnetic" position) and of comparable magnitude to the p-H isotropic shift. This change in sign of the isotropic shift is characteristic of π-spin delocalization[39] and is caused by direct delocalization of parallel spin from the aromatic ring into the π-symmetry orbital of the Me fragment. The temperature dependences of the resonances of the three complexes all show Curie behavior, i.e., the isotropic shifts increase with decreasing temperature.

Summary and Conclusions. Brief exposure of MeCN solutions of $[VOX_4]^{2-}$ (X = Cl, Br) and RCO_2^- salts to air provides a convenient synthetic route to $[V_5O_9X(O_2CR)_4]^{2-}$ complexes; a related reaction in the presence of $AgNO_3$ gives a $[V_4O_8(NO_3)(O_2CR)_4]^{2-}$ product. These complexes are all mixed-valent V^{IV}/V^V and possess interesting structures and properties. The discovery of ferromagnetic exchange interactions between the V^{IV} ions of the pentanuclear complexes provides rare examples of high spin values in the ground state for V^{IV}_x species: it is noteworthy that if the proposed rationalization of the ferromagnetic interactions is correct, the diamagnetic V^V ion is of great importance to the observed magnetic properties of the complexes even though it itself is, of course, diamagnetic (d^0) and therefore ostensibly of no importance to the magnetochemistry. Indeed, the results obtained in this work suggest that other mixed-valent V^{IV}/V^V polynuclear complexes with appropriate topologies may be a good source of additional ferromagnetically-coupled systems with large ground state spin values.

The spectroscopic studies show that the pentanuclear complexes retain their solid-state structures on dissolution in MeCN, and indicate that the isotropic shifts observed in ^{1}H NMR spectra are contact in origin *via* a π spin delocalization mechanism, as might be expected for spin density in V d_π orbitals. The EPR spectrum of $[V_4O_8(NO_3)(tca)_4]^{2-}$ is particularly noteworthy, yielding a remarkably well-resolved hyperfine structure consisting of 29 lines assignable to hyperfine interactions with four equivalent ^{51}V nuclei and indicating electron delocalization or de-trapping that is fast on the EPR time scale at room temperature.

The present work represents the initial results of our efforts in V carboxylate chemistry at the V^{IV}/V^V level and complements our recent report of a tetranuclear V^{III} carboxylate species.[19] A number of additional results and new species have since been prepared and are currently under study, and these will be reported in due course.

Acknowledgment. This work was supported by the U. S. Department of Energy, Office of Basic Energy Sciences, Division of Chemical Sciences, Grant ER 13702 (G.C.), and by the National Science Foundation, Grant CHE-9420322 (D.N.H.).

Supporting Information Available: Textual summaries of the crystallographic data collections and structure solutions, tables of atomic coordinates, thermal parameters, and bond distances and angles, and fully labeled figures for complexes **4a**·MeCN, **6b**, and **7**·H_2O (50 pages). Ordering information is given on any current masthead page.

IC9605938

(39) *NMR of Paramagnetic Molecules*; LaMar, G. N.; Horrocks, W. D., Jr., Holm, R. H., Eds., Academic Press: New York, 1973.